

Contents lists available at [ScienceDirect](http://www.sciencedirect.com)

Journal of the Mechanical Behavior of Biomedical Materials

journal homepage: www.elsevier.com/locate/jmbbm

Constitutive modeling of jugular vein-derived venous valve leaflet tissues



Nayyan Kaul, Hsiao-Ying Shadow Huang*

North Carolina State University, Department of Mechanical and Aerospace Engineering, R3158 Engineering Building 3, Campus Box 7910, 911 Oval Drive, Raleigh, NC 27695, USA

ARTICLE INFO

Keywords:

Constitutive model
Phenomenological model
Venous valve
Chronic venous insufficiency
Biaxial testing
Biomechanics

ABSTRACT

Venous valve tissues, though used in vein reconstruction surgeries and bioprosthetic valves with moderate success, have not been extensively studied with respect to their structure. Their inherent anisotropic, non-linear behavior combined with severe diseases which affect veins, such as chronic venous insufficiency, warrant understanding the structure and material behavior of these tissues. Hence, before any bioprosthetic grafts may be used in place of tissues, it is of the utmost importance to understand the mechanical and structural properties of these tissues as this may lead to higher success rates for valve replacement surgeries. The longevity of the bioprosthetics may also increase if the manufactured grafts behave the same as native valves. Building on the scant information about the uniaxial and biaxial mechanical properties of jugular venous valves and wall tissues from previous studies, the current focus of our investigation lies in understanding the material behavior by establishing a phenomenological strain energy-based constitutive relation for the tissues. We used bovine veins to study the behavior of valve leaflet tissue and adjoining wall tissue (from the proximal and distal ends of the veins) under different biaxial testing protocols. We looked at the behavior of numerical partial derivatives of the strain energy to select a suitable functional form for the strain energy for wall and valve tissues. Using this strain energy descriptor, we determined the Cauchy stress and compared it with experimental results under additional sets of displacement-controlled biaxial testing protocols to find material specific model parameters by the Powell's method algorithm. Results show that whereas wall tissue strain energy can be explained using a polynomial non-linear function, the valve tissue, due to higher non-linearities, requires an exponential function. This study may provide useful information for the primary stages of bioprosthetic designs and replacement surgeries and may support future studies investigating structural models. It may also support the study of valvular diseases by providing a way to understand material properties and behavior and to form a continuum model when required for numerical analyses and computational simulations.

1. Introduction

The venous valves regulate retrograde blood flow, among other important functions (Gottlob and May, 1986). Parietal valves, also called pocket valves, are the most common venous valves and are found attached to the walls of the veins in a bicuspid, or occasionally tricuspid, manner. In this way, the valves function in a similar fashion to aortic or mitral valves. Aortic valves and venous valves contain similar extracellular matrix (i.e., constituents and microstructure) but exhibit different mechanical and biochemical properties (Ackroyd et al., 1985; Humphrey, 2002; Huang and Lu, 2017). The structure, orientation, density, and diameters of collagen fibers in the tissue are largely responsible for determining tissue anisotropy. One visible difference between the two is the thickness of venous valves, which is much less than that of heart valves (e.g., 50 μm for bovine venous valve vs. 1500 μm for bovine heart valve (Masoumi et al., 2013)).

When dealing with the mechanics of soft tissues, their complex mechanical properties require more descriptive constitutive laws than simple metals and rubber (Treloar, 1943a, 1943b, 1946). Many previous studies have provided descriptors for different soft animal tissues (Nolan et al., 2014) like aortic valves (May-Newman et al., 2009), arterial walls (Holzapfel et al., 2004; Humphrey, 1999), myocardium (Humphrey et al., 1990a, 1990b), the cornea (Nguyen et al., 2008), etc. Because aortic valves and wall tissue are responsible for a number of heart diseases and deaths annually, this is an important topic to study in the field of bioprosthetics. However, its venous counterpart, the venous valves, which are commonly used as replacement grafts and are also involved in diseases such as vein thrombosis (Eberhardt and Raffetto, 2005; Gottlob and May, 1986; Vogel et al., 2012), varicose veins (Edwards and Edwards, 1940; Gottlob and May, 1986), and chronic venous insufficiency (Bergan, 2008; Bernardini et al., 2010; Gottlob and May, 1986), does not garner as much attention. With the scant

* Corresponding author.

E-mail address: hshuang@ncsu.edu (H.-Y.S. Huang).

<http://dx.doi.org/10.1016/j.jmbbm.2017.06.037>

Received 17 April 2017; Received in revised form 23 June 2017; Accepted 28 June 2017

Available online 01 July 2017

1751-6161/ © 2017 Elsevier Ltd. All rights reserved.

information available on the mechanical behavior of venous valves, it is difficult to decide analytically if any other man-made material or animal tissue will be a good fit as a graft.

A variety of pathological processes affect the proper functioning of venous valves, such as coagulation of blood in the sinus and over-dilation (Buescher et al., 2005) of the vein due to higher hydrostatic pressure (Bergan, 2008; Eberhardt and Raffetto, 2005; George, 2012). Also, venous wall weakness has been attributed to hereditary reasons (Gottlob and May, 1986). To understand how wall tissue, along with the valve tissue, is responsible for valve incompetency, we need to have a full understanding of the mechanics of healthy wall tissue which warrants testing the avaluvar wall region in addition to healthy venous valves.

Soft tissues, due to their inherent properties, are modeled as hyperelastic materials, which reduces to providing a strain energy expression for material characterization. These material specific laws are either data driven or are constrained by microstructural level interactions in the material. The first kind of models are called phenomenological models. The material is subjected to various types of loading scenarios to investigate its behavior experimentally. The aim then lies in trying to describe all observed behavior using a single model. The structural models, however, are motivated by the microstructure of the material. They seek to explain the material behavior by taking into account the interactions at the structural level. They are not simply data driven, but have established a concrete foundation in the form of differential equations and probability functions which explain the structure. Structural models are difficult to implement in a finite element analysis environment due to their complex nature, while phenomenological models have a certain number of parameters which are simple to implement.

There are quite a few studies in the field which present several models following different approaches. Most phenomenological models such as those employed by Mooney-Rivlin (Mooney, 1940; Rivlin, 1948a, 1948b; Rivlin and Saunders, 1951), Ogden (1972), Shariff (2000), and Gent (Gent, 1996; Gent and Thomas, 1958) tend to focus on isotropic materials, whereas structural models like that used by Arruda (Arruda and Boyce, 1993) or Holzapfel (Holzapfel et al., 2000, 2004) are quite difficult to implement and require a detailed structural survey of the specimen with probability distributions explaining the orientations of fibers. There are currently no studies on constitutive models describing venous valvular tissue remodeling and thus no means of predicting the structural basis for potential tissue failure. Therefore, for a pilot study, it is important to characterize the tissue behavior on a phenomenological basis.

Currently, only a single study by Ackroyd et al. (1985) has reported mechanical properties of venous valve leaflet tissue, and that only dealt with uniaxial tensile strength and failure strain. In an effort to refine tissue-level principles of venous valve function and valve replacement, Huang and Lu began characterizing the biaxial non-linear mechanical behavior of venous valve leaflet tissue (Huang and Lu, 2017). This study laid the foundation and was critical to understanding valve opening and closing mechanisms in healthy and diseased veins, while also providing guidance in designing not only native-like venous valve replacements, but venous-derived bioprosthetic heart valves as well. Based on the study by Huang and Lu (2017), as is typical for many soft collagenous tissues, three distinct stress-strain response regions were evident for the venous valves: a relatively linear, low tangent modulus toe region between 0% and 25% strain, an exponential transition region between 25% and 45% strain, and a higher tangent modulus, relatively linear region between 45% and 60% strain. It was also observed that beyond the peak applied strain, tissue starts to tear. Because soft tissues behave differently under various external conditions, the stress-strain curves reported from any study are generally limited by the testing range. Therefore, it is important to formulate a unique constitutive equation to completely describe the mechanical behavior of venous valve tissues.

To that end, the objective of our current study lies in understanding the material behavior by selecting a phenomenological strain energy-based constitutive relation which can closely predict the mechanical behavior of the tissues. A comparative study between the behavior of valve leaflet tissue and adjoining wall tissue was conducted to study the degree of anisotropy in both (if any). The selection of the strain energy descriptor in the study is guided purely by experimental data from a variety of biaxial experiments over a wide range of deformations. After selecting the model descriptor, we estimated the material parameters for the experiments which are required to implement the model in the finite element analysis environment for simulations. This study can provide useful information by offering a deeper insight into the mechanical behavior of soft tissues and in primary stages of bioprosthetic designs, replacement surgeries, and for studying valvular damages due to diseases.

2. Materials and methods

2.1. Preliminaries and modeling

Structural exploration studies on jugular venous tissues have shown that this tissue has an incompressible homogeneous structure as valve tissues are found to have bundles of aligned collagen fibers (Gottlob and May, 1986; Huang and Lu, 2017) throughout the tissue embedded in extra cellular matrix. However, the belly region of the valve has consistently more homogeneous structure compared to the commissures or attachment area. A few studies which investigated the mechanical behavior of jugular venous tissue indicate non-linear and anisotropic behavior in the valve and wall tissue, the valve having more non-linearities. The study by Huang and Lu (Huang and Lu, 2017; Lu, 2016) concluded by identifying the high non-linearity and anisotropic nature of jugular vein valves based on equibiaxial testing, by providing three different, relatively linear, tangent modulus regimes over the strain range of 0–60% followed by sample tearing at strains ranging from 65% to 80% resulting from sample to sample variability. Moreover, the histological study for the valves presented in the study also indicated the local transversely isotropic nature of the venous valves in the test region (Huang and Lu, 2017). This information enables us to plausibly assume that the tissue under study, valve and wall alike, are pseudoelastic, incompressible, homogeneous, and locally transversely isotropic with respect to fiber axis.

Soft tissues that behave in this manner are categorized as hyperelastic and a strain energy expression is adequate to constitutively describe the behavior of these tissues. As suggested by Humphrey et al. (1990a, 1990b), for modeling a hyperelastic soft tissue with this type of behavior and preserving the simplicity of the experimental testing involved, it is plausible to assume a strain energy expression which is a function of only two invariants of the deformation, i.e. I_1 and α .

$$W = W(I_1, \alpha),$$

where I_1 is the first invariant of the right Cauchy-Green deformation tensor \mathbf{C} and $\alpha^2 = I_4$, which is the fourth invariant of the right Cauchy-Green deformation tensor \mathbf{C} .

$$I_1 = \text{trace}(\mathbf{C})$$

and

$$\alpha^2 = I_4 = \mathbf{N} \cdot \mathbf{C} \cdot \mathbf{N},$$

and \mathbf{N} is the unit vector in the direction of the fiber axis.

Using these assumptions, the general constitutive statement for Cauchy stress for the material becomes:

$$\mathbf{t} = -p\mathbf{I} + 2W_1\mathbf{B} + \left(\frac{W_\alpha}{\alpha}\right)\mathbf{F} \cdot \mathbf{N} \otimes \mathbf{N} \cdot \mathbf{F}^T, \quad (1)$$

where \mathbf{t} is Cauchy stress, \mathbf{B} is the left Cauchy-Green deformation tensor, \mathbf{F} is the deformation gradient, \mathbf{I} is the identity tensor, p is the Lagrange

multiplier to enforce incompressibility, and W_I and W_α are the partial derivatives of the strain energy expression with respect to the two coordinate invariants: $W_I = \frac{\partial W}{\partial I_1}$ and $W_\alpha = \frac{\partial W}{\partial \alpha}$. A strain energy descriptor characteristic to the tissue under study, along with the general constitutive statement, completes the hyperelastic model. The strain energy descriptor is decided on the basis of experimentation which involves biaxial testing where each invariant is alternatively held at a constant value, called “constant invariant testing.” The plots of W_I and W_α with respect to the invariants, termed “response curves,” provide an empirical basis to decide a suitable function for the strain energy descriptor.

2.2. Tissue procurement and preparation

Due to issues associated with procuring and testing human tissues, and the fact that bovine tissues are used on a large scale as a suitable substitute from a medical point of view in bioprosthetic grafts, we used tissue samples from a number of mature bovines of Holstein breed, 10+ years old with an approximate weight of 1250 lbs. to incorporate and examine any biological variability which may arise. A total of 24 bovine veins in a bag of ice-cold Hank’s balanced salt solution (HBSS; Lonza, Walkersville, MD) with Gibco® Antibiotic-Antimycotic (Thermo-Fisher Scientific, Waltham, MA) were shipped overnight on ice, ~24 h post-slaughter. Wall tissues were dissected from proximal and distal end of 8 veins, and 32 valvular tissues are dissected from 16 veins. Test specimens are cut from the belly region of the valve and avalvular region of the wall in square sections of 7–10 mm per side and stored in HBSS. It is important to note that wall tissue test specimens are not taken from the sinus region of the valve owing to any fatigue they might have undergone during their life.

2.3. Testing methods and protocols

A detailed description of the biaxial testing device has been previously presented (Huang et al., 2012; Huang and Huang, 2015). As discussed in Huang and Lu (Huang et al., 2012; Huang and Lu, 2017), the tissue test specimens were mounted on the biaxial testing (CellScale Biomaterials Testing, Waterloo, ON, Canada) using rakes in a bath of HBSS pre-heated to 37 °C to imitate physiological conditions. For the current study, the effective central region subject to stretching is 4.5 mm × 4.5 mm. The test rig has two load cells (10 N ± 0.02 N) mounted perpendicular to each other and two actuators opposite to the load cells to simulate loading or stretching. The displacement of the actuators is recorded along with the load cell readings. Using sutures and hooks for stretching the soft tissue can lead to inaccurate data due to sagging of the thread. However, using rakes eliminates this issue (Eilaghi et al., 2009, 2010; Nolan and McGarry, 2016).

The mounting of the specimen is set up in such a way that the fiber axis for the tissue samples (the direction along which most fibers are oriented: axial for wall tissue and circumferential for the valve tissue (Gottlob and May, 1986)) coincides with one of the loading axes (x-axis

in the protocol). Specimen mounting and the fiber alignment with the loading axes of the biaxial testing could refer to Huang et al. (2012). Fiber angle – the angle between the loading axis and the high fiber alignment axis – is crucial for determining the mechanical behavior of the tissue. Mounting the tissue as defined above reduces the fiber angle to zero, which in the absence of shear simplifies the calculations of I_4 and in turn α . Great care is taken to ensure that the arms of one rake are aligned with those mounted opposite to it to avoid any shear stress which might be generated during the planar testing due to misalignment of the rakes. The test specimen is preconditioned with a preload of 10 mN for eight loading-unloading cycles up to 30% strain at a strain rate of 1% per second followed by a rest period of 300 s.

Thickness of each tissue sample is recorded four to five times before testing by using a dial gauge (± 0.0001 in., The L.S. Starrett Co., Athol, MA) and then an average value is used for stress calculations. Length along each side is taken from the effective area between the rakes. The stretch is calculated from the displacement data and the first Piola-Kirchhoff stress (i.e., recorded force at any instance/original loading area) is calculated from the force data (Nolan and McGarry, 2016) which is converted into Cauchy stress (recorded force at any instance/loading area at any instance) using deformation gradients (Fung, 1965; Slaughter, 2001). The underlying kinematic assumptions for this are that of homogeneous planar biaxial testing and can be found in the study by Humphrey et al. (1990a).

In order to select a suitable strain energy descriptor expression, we needed some experimental basis for the selection in terms of response curves generated from constant invariant testing. The testing procedure incorporates one invariant constant during the deformation and observing how W_I and W_α behave with the other changing invariant. Based on the approximate mechanical breaking strength of the valve tissue at about 60% (Huang and Lu, 2017), we selected the testing range of I_1 and α . Positing an approximate 60% true strain breaking strength, we tested the samples for $3.2 < I_1 < 4.4$ and $1.1 < \alpha < 1.7$. The complete testing protocol including preconditioning of the sample is shown in Fig. 1.

Constant α tests involve keeping the fiber direction stretch at a constant value and stretching and un-stretching the orthogonal axis in a triangular fashion, whereas constant I_1 inherently requires one stretch to increase and the other to decrease at the same time in order to keep I_1 at a constant value. The protocol shown in Fig. 1 was subdivided into two groups to prevent accumulation of damage at higher strains affecting the following low strains and for cleaner presentation of data: a “lower strain set” with maximum stretch < 1.5 and a “higher strain set” with maximum stretch > 1.5. A total of 16 wall samples – eight from the distal end of the vein and eight from the proximal end of the vein – along with eight samples of valve tissue were tested under this protocol. The force-displacement data as measured by the test equipment are then converted into W_I , W_α , I_1 and α to obtain the response curves using formulae presented by Humphrey et al. (1990a, 1990b). The main purpose of the response curves was to discern the behavior of the strain energy function to guide the selection of an empirical strain energy

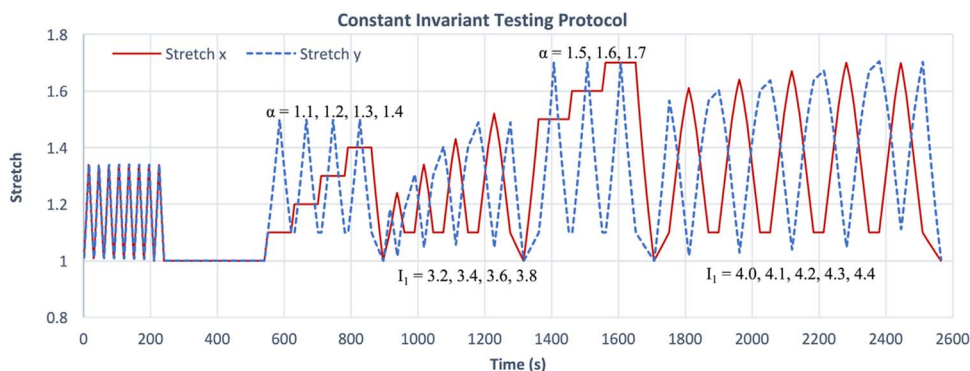


Fig. 1. Profile of stretch vs time in orthogonal directions for constant invariant testing.

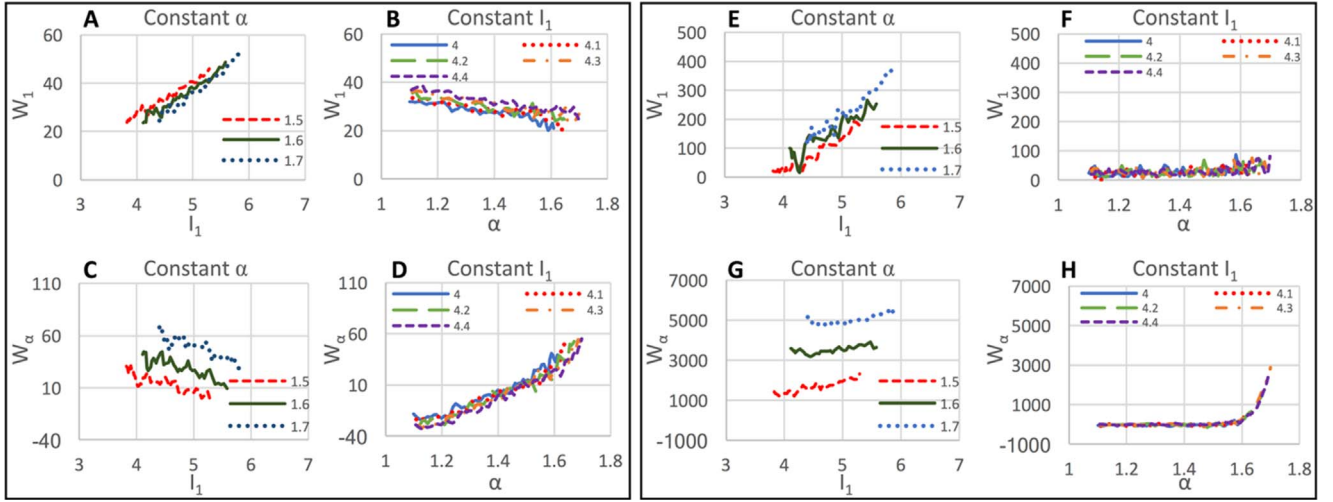


Fig. 2. Response curves for wall (A-D) and valve (E-H) samples where strain energy derivatives are presented in kPa. Panel A shows the variation of W_{I_1} with I_1 at constant values of α which are shown using three different colors. Same legend is used in Panel E, C and G. Similarly, curves for 5 values of I_1 are shown in Panels C, D, F and H.

relation. However, the model parameters were calibrated using separate set of equibiaxial and off-axis tests.

2.4. Model parameters

One of the main principles of pseudoelasticity is that the tissues may have different properties during the loading and unloading cycle (Fung, 1993). We observed qualitatively that the sample behaved similarly during loading and unloading with some hysteresis. Thus, assuming that same functional form of the descriptor can be used for loading and unloading with different material parameter sets, we present the material model results calibrated for the loading portion of the equibiaxial and off biaxial testing in the current study. It is important to note that Constant I_1 tests cannot be used for such calibration due to the inherent nature of the test and therefore, Constant invariant tests were not used at all for parameter estimation. Fig. 2 shows the response curves generated during the loading phase for a selected wall sample from the distal end of the vein and a valve sample for the “higher strain set” (i.e., maximum stretch greater than 1.5 for both directions) using the experimental data from constant invariant tests. The response curves for the “higher strain set” as well as “lower strain set” showed similar behavior of strain energy derivatives with respect to the invariants. Therefore, we reported higher strain set part of the experimental study and interested readers are referred to Kaul (2016) for response curves on the “lower strain set.” Graphs A and C (or E and G) of Fig. 2 represent the variation of W_{I_1} and W_{α} with respect to I_1 for constant values of α mentioned in the index (i.e., $\alpha = 1.5, 1.6,$ and 1.7) for the wall (or valve) tissue samples. Similarly, Graphs B and D (or F and H) of Fig. 2 represent the variation of W_{I_1} and W_{α} with respect to α for all constant I_1 tests (i.e., $I_1 = 4.0, 4.1, 4.2, 4.3,$ and 4.4) for wall (or valve) tissue samples. A functional form for the strain energy descriptor was then obtained from the behavior of strain energy derivatives in the response curves.

By examining the qualitative behaviors of these curves in Fig. 2, it can be seen that all the curves in panels A-C and E-G are approximately linear, while those in panels D and H are not. However, the non-linear relationship between W_{α} and α in panel D of Fig. 2 for the wall tissue samples can be better described using a second-order polynomial. The curves in panel H of Fig. 2 for the valve tissue samples are highly non-linear and it can be seen upon examination of the slope of the curve that it is exponential in nature. Note that all eight valve tissue and 16 wall tissue samples exhibited similar qualitative behavior in their response curves, as shown above. Based on these observations, we found that a five-parameter polynomial type strain energy descriptor given by

Humphrey et al. (1990a, 1990b) for the wall tissue and a three-parameter exponential type function given by May-Newman and Yin (1998) for the valve tissue were the closest matching phenomenological models in the literature which can explain the behavior of the tissues which are shown in Eqs. (2) and (3).

$$W^{wall} = c_1(\alpha-1)^2 + c_2(\alpha-1)^3 + c_3(I_1-3) + c_4(I_1-3)(\alpha-1) + c_5(I_1-3)^2 \quad (2)$$

$$W^{valve} = c_0(\exp(c_1(I_1-3)^2 + c_2(\alpha-1)^4) - 1) \quad (3)$$

The restrictions applied to the parameters require all parameters to be positive except for c_4 of W^{wall} , which is negative, stemming from the negative slopes of the curves in panels B and C of Fig. 2. For further clarification, interested readers are referred to the study published by Humphrey et al. (1990a, 1990b).

After selecting the descriptor function, the next step of the modeling process requires finding material parameter values (five for W^{wall} and three for W^{valve}). Best fit values are obtained for each sample separately by minimizing the sum of the squares of the residuals (Yin et al., 1986) using the Powell's method algorithm (Press et al., 1992). The residual is defined as the error between the experimental measured and theoretically predicted Cauchy stress.

$$\chi^2 = \sum_{i=1}^n [y^i - t^i]^2$$

Here y^i is stress at the i th data point, and t^i is the Cauchy stress from the fitted function evaluated at the corresponding stretch ratio. For model predicted stress, the expressions can be found by substituting the energy descriptor in the general constitutive relation in Eq. (1). Model predicted stress expressions for polynomial type descriptors from Eq. (2) are as follow:

$$\begin{aligned} \mathbf{t}_{11}^{wall} &= 2(\lambda_1^2 - \lambda_3^2)[c_3 + c_4(\alpha-1) + 2c_5(I_1-3)] \\ &\quad + \lambda_1[2c_1(\alpha-1) + 3c_2(\alpha-1)^2 + c_4(I_1-3)] \\ \mathbf{t}_{22}^{wall} &= 2(\lambda_2^2 - \lambda_3^2)[c_3 + c_4(\alpha-1) + 2c_5(I_1-3)] \end{aligned} \quad (4)$$

Similarly, the expressions for model predicted stress for the exponential model in Eq. (3) were calculated as:

$$\begin{aligned} \mathbf{t}_{11}^{valve} &= (4c_0c_1(\lambda_1^2 - \lambda_3^2)(I_1-3) \\ &\quad + 4c_0c_2\lambda_1(\alpha-1)^3)\exp[c_1(I_1-3)^2 + c_2(\alpha-1)^4] \\ \mathbf{t}_{22}^{valve} &= 4c_0c_1(\lambda_2^2 - \lambda_3^2)(I_1-3)\exp[c_1(I_1-3)^2 \\ &\quad + c_2(\alpha-1)^4] \end{aligned} \quad (5)$$

For parameter estimation, a separate set of biaxial testing was

conducted in which separate preconditioned tissues were subjected to four off-axial and one equibiaxial stretching protocol consecutively (in the order of Axial: Circumferential [A:C] for wall tissue samples or Circumferential: Radial [C:R] for valve tissue sample = 2:1, 1:2, 1.5:1, 1:1.5, 1:1) where the ratio indicates the ratio of strains in the orthogonal directions. A maximum of 70% true strain was selected for this phase of biaxial testing.

For each tissue sample, a combination of three test protocols (equibiaxial A:C or C:R = 1:1, off-axis A:C or C:R = 1:1.5, off-axis A:C or C:R = 1.5:1) were used to determine the material parameters of t^{wall} and t^{valve} (Eqs. (4) and (5)). A total of 70 data points from fiber and cross-fiber directions were taken for each protocol. R-squared values are used to determine the level of fitness of the model to the data.

Convergence of the parameters was verified by using a range of initial values for around two orders of magnitude for each coefficient. For higher magnitude initial hypotheses, the algorithm was still converging to the same material parameters but required multiple runs due to local minima wells. To ensure that the material model is not over-parameterized, we calculated the correlation matrix and ensured the determinant of the matrix as well by checking if any unity element is present in the matrix (Kaul, 2016).

To ensure the usefulness of the constitutive relation, we looked into the predictive capability of the material parameter model. For this, we evaluated how well the material parameters (determined from three different protocols – 1:1, 1.5:1, 1:1.5) could predict the data from two other off-axis protocols (1:2 and 2:1), which were not used, to find the material parameters. In addition, a single representative group of parameters (i.e., combined parameters) is also presented for each wall (proximal and distal) and the valve tissue samples using the individual material sets.

3. Results and discussion

As with the constant invariant testing, a total of 16 wall samples (eight distal and eight proximal) and eight valve tissue samples underwent biaxial testing. Best-fit parameters were calculated using the methods discussed in the previous section. Table 1 shows the values of five material parameters in polynomial type strain energy function for all 16 samples of wall tissue. Table 2 shows the three parameters for the exponential model along with correlation coefficients for all the valve samples tested. High correlation coefficients for each sample indicate

Table 1

Material parameters for 16 samples of wall tissues along with one set of representative parameters (i.e., combined parameters) for each proximal wall tissue and distal wall tissue. All constants have units of kPa.

| Sample | C ₁ | C ₂ | C ₃ | C ₄ | C ₅ | R _x | R _y |
|--------------------------------|----------------|----------------|----------------|----------------|----------------|----------------|----------------|
| W01D | 47.19 | 14.38 | 8.94 | -13.64 | 4.26 | 1.00 | 0.99 |
| W02D | 26.50 | 16.39 | 3.40 | -8.32 | 2.67 | 0.99 | 0.98 |
| W03D | 29.76 | 33.68 | 12.34 | -9.90 | 3.82 | 1.00 | 0.99 |
| W04D | 4.25 | 32.30 | 11.52 | -9.87 | 3.56 | 1.00 | 1.00 |
| W05D | 4.67 | 26.04 | 12.95 | -13.31 | 4.68 | 1.00 | 1.00 |
| W06D | 5.60 | 26.25 | 6.18 | -14.31 | 3.72 | 0.99 | 0.98 |
| W07D | 6.43 | 111.92 | 4.72 | -32.12 | 7.68 | 0.93 | 0.94 |
| W08D | 17.06 | 16.31 | 10.81 | -8.90 | 3.19 | 1.00 | 0.99 |
| Combined parameters (Distal) | 9.49 | 42.58 | 7.75 | -15.59 | 4.46 | - | - |
| W01P | 43.74 | 19.70 | 6.91 | -10.71 | 4.04 | 1.00 | 0.99 |
| W02P | 12.16 | 21.07 | 7.18 | -7.30 | 2.19 | 0.99 | 0.98 |
| W03P | 30.08 | 31.97 | 0.10 | -9.12 | 3.09 | 0.99 | 0.98 |
| W04P | 0.10 | 18.66 | 0.10 | -0.44 | 3.20 | 0.91 | 0.86 |
| W05P | 3.62 | 21.27 | 2.71 | -10.82 | 3.43 | 0.98 | 0.99 |
| W06P | 75.74 | 48.19 | 0.12 | -58.47 | 12.25 | 0.96 | 0.83 |
| W07P | 13.73 | 58.34 | 0.10 | -32.87 | 9.93 | 0.96 | 0.94 |
| W08P | 7.90 | 73.26 | 0.10 | -32.93 | 6.97 | 0.92 | 0.80 |
| Combined parameters (Proximal) | 30.66 | 27.96 | 1.97 | -17.92 | 5.21 | - | - |

Table 2

Material parameters for eight samples of valve tissues along with one set of representative parameters (i.e., combined parameters). C₀ has the units of kPa and C₁, C₂ are dimensionless.

| Sample | C ₀ | C ₁ (× 10 ⁻²) | C ₂ (× 10 ⁻²) | R _x | R _y |
|---------------------|----------------|--------------------------------------|--------------------------------------|----------------|----------------|
| V01 | 472.70 | 4.30 | 34.00 | 0.95 | 0.93 |
| V02 | 25.76 | 6.10 | 106.60 | 0.95 | 0.93 |
| V03 | 185.43 | 7.10 | 30.30 | 0.90 | 0.93 |
| V04 | 295.66 | 7.70 | 20.40 | 0.90 | 0.90 |
| V05 | 66.83 | 3.70 | 185.90 | 0.97 | 0.71 |
| V06 | 132.79 | 7.90 | 61.30 | 0.95 | 0.96 |
| V07 | 40.36 | 4.40 | 170.70 | 0.96 | 0.75 |
| V08 | 42.57 | 2.90 | 146.20 | 0.97 | 0.67 |
| Combined parameters | 112.28 | 5.90 | 109.00 | - | - |

how well the model predicts the experimental data. Fitting for three testing ratios (i.e., 1:1, 1.5:1, 1:1.5) for one sample for each wall and valve is shown in Fig. 3. Stress-stretch data along with the model fitting for one of the wall tissue sample (W03D) is shown in Fig. 3A,C,E for the three testing ratios, respectively. The axial direction appears to be stiffer in all the cases with excellent model fitting. Correlation coefficients listed in Table 1 for the wall samples are evidence of good fit for the wall tissue using the polynomial model W^{wall} . The presence of a stiffer axial direction is always indicative of less interdependence of properties between two orthogonal directions (i.e., axial and circumferential directions), irrespective of the loading ratio, and thus suggests a more aligned, unidirectional network structure.

Fig. 3B,D,F shows the comparison between the experimental data and model predicted stress for one of the valve tissue (V01) for the three test ratios. While the exponential type model W^{valve} is an acceptable qualitative fit, quantitatively a prediction error of about 2 MPa at a stretch value of 2 can be seen in Fig. 3D. It may also be noted that for the valve tissue, radial directional properties take over and become stiffer than in the circumferential direction, when the stretch in the circumferential direction is increased (i.e. i.e. C:R = 1.5:1 and 2:1 in Fig. 3F and Fig. 3H). This behavior points toward the intertwined nature of fibers in the valves, instead of a single directional alignment. The predictive ability of the parameters was checked by using the parameters from Tables 1 and 2 to predict the other two sets of off-axis test data (i.e., 1:2, 2:1) which were not used in the parameter estimation. The predictive capability for the same two samples is also shown in Figs. 3G-3J.

As can be seen from the fits and the correlation coefficient values, the polynomial type function is an almost perfect model to predict the behavior of the wall tissue (Figs. 3G and 3I; Table 1, R_x = 0.95 and R_y = 0.98), whereas the exponential model used for valve tissue predicts the qualitative nature of the behavior but shows a large amount of prediction error in the fits (Figs. 3H and 3J; Table 2, R_x = 0.17 and R_y = 0.55). In terms of predictive ability, it has a consistent error in the circumferential direction.

The response curves for the wall (Fig. 2A-D) match very well to the ones in the study by Humphrey et al. (1990a), but the response curves for the valve, while exponential in nature, have some notable differences from the ones presented by May-Newman and Yin (1998) for mitral valve. Hence, the prediction error suggests intrinsic biological differences between arterial and venous systems which might be the result of macro logical structural differences and are worth future exploration.

Material parameters provided from our study for venous valve tissue differ from ones given by May-Newman for mitral valves (May-Newman and Yin, 1998) by an order of 10² – 10³ and by an order of 10⁴ from the parameters given for aortic valve tissue (May-Newman et al., 2009). The wide differences with respect to aortic and mitral valves can be attributed to the wide disparities in the maximum achievable stress values (5–6 kPa for aortic valves, 0.2–0.6 MPa for mitral valves, and 3–6 MPa for venous valves), but the stark difference lies in the response

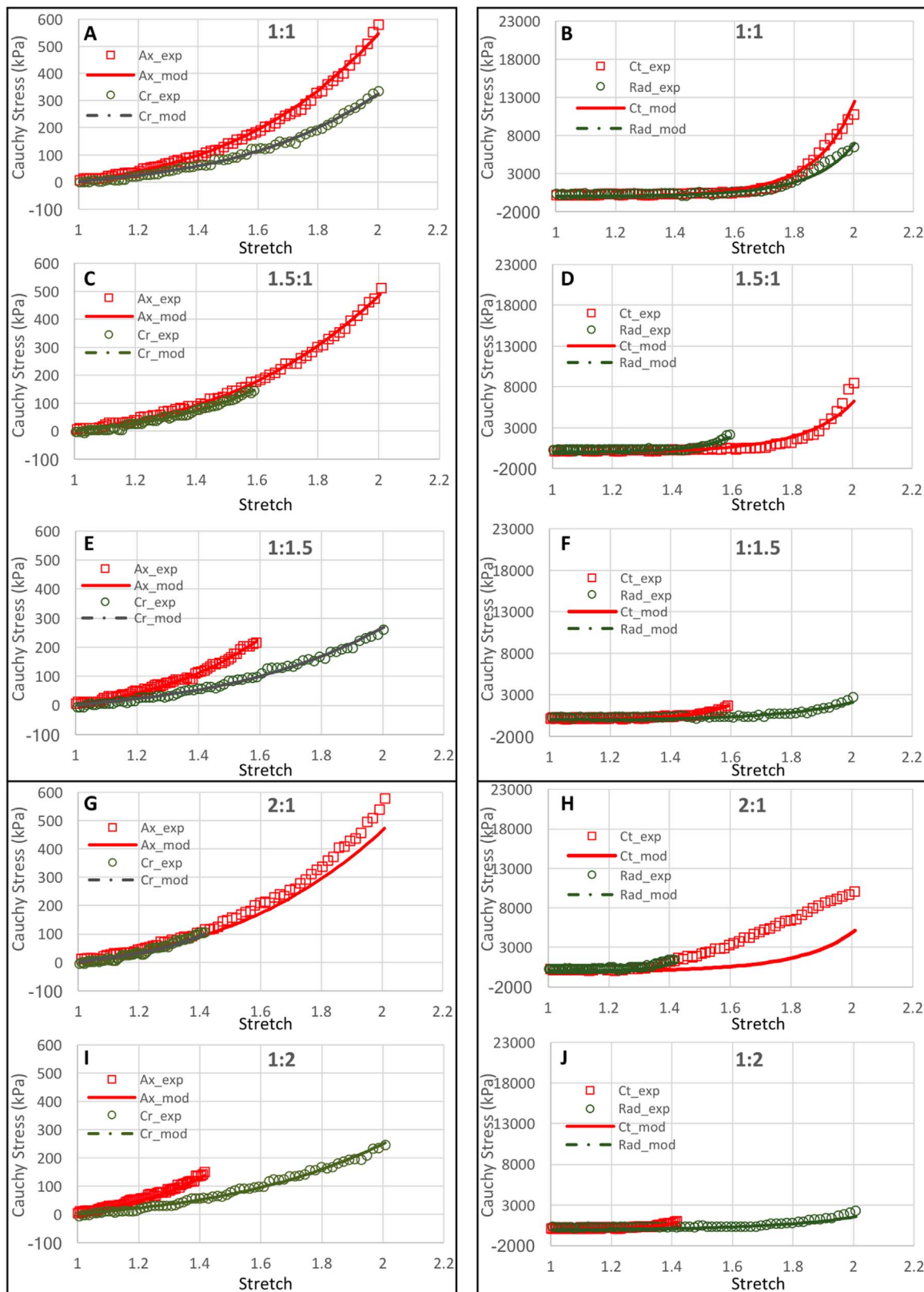


Fig. 3. Plot of Cauchy stress vs stretch along with the fits using the individual material parameters for wall tissue (left) and a valve tissue (right). Experimental data for fiber direction (axial [Ax] for wall tissue and circumferential [Ct] for valve tissue) is shown using square markers along with a solid fit line. Cross-fiber direction is shown using circular markers with a dashed fit line (circumferential [Cr] for wall tissue and radial [Rad] for valve tissue). Subplots present data for separate biaxial tests.

curves observed between venous valves and aortic (or mitral) valves. The mitral valve response curves have an exponential variation of W_1 and W_a with both invariants at a low stretch range, whereas in the case of venous valves, only W_a has such an exponential rise at stretches

higher than 1.5 (Fig. 2H). Moreover, W_1 behaves almost linearly with I_1 for venous valves but exponentially for aortic (May-Newman et al., 2009) (or mitral (May-Newman and Yin, 1998)) valves. This might indicate a large sudden uncramping of fibers in the case of mitral valves

as compared to venous valves, whereas strain energy has more dependence on the extent of deformation (I_1) in mitral valves than in venous valves, which can indicate a more plastic behavior of mitral valves as compared to venous valves.

It is possible that the same exponential model with different exponents for I_1 and α may provide better fitting results, though this was outside the scope of the present study. However, these results indicate that our assumption of fiber alignment in one direction (axial for wall and circumferential for valve) holds good for the wall tissues whereas for the valve, we deduce that the fibers might not be as highly aligned as they are in the cases of wall or aorta valves. Instead, the fibers may have a more entangled web-like structure. We began further investigation on the jugular valve leaflet microstructure tissue using immunohistology and confocal microscopy. Using the polynomial model for the wall, we compared the strain energy levels between proximal and distal wall tissues at the same stretch level. In all of the testing ratios (equibiaxial or off-axial), we observed that the distal wall tissue samples have more strain energy density per unit volume, which indicates higher forces at the distal end as compared to the proximal end. This may be attributed to the higher hemodynamic pressure at the distal end of the vein.

Due to growing research groups in computational tissue mechanics, and Fung's model to describe soft tissue mechanics has become one of available materials laws from a commercialized finite element package (i.e., ABAQUS FEA, Providence, Rhode Island). We also conducted force-controlled experiments (C:R = 1:1, 3:1, 1:3) by using the rest of 24 valves, in addition to the three-parameter exponential model for jugular valve leaflets. The experimental and modeling procedures are detailed in Billiar (Billiar and Sacks, 2000), Sun (Martin and Sun, 2014; Sun and Sacks, 2005), and Huang (Huang, 2004). We fitted measured data with the most widely acceptable 10-parameter Fung's exponential mode (Eq. 6).

$$W = \frac{C}{2}(e^Q - 1)$$

$$Q = A_1 E_{11}^2 + A_2 E_{22}^2 + 2A_3 E_{11} E_{22} + A_4 E_{12}^2 + A_7 E_{33}^2 + 2A_8 E_{11} E_{33} + 2A_9 E_{22} E_{33} + A_{10} E_{13}^2 + A_{11} E_{23}^2 \tag{6}$$

Using the correlation coefficient as the quantitative measure, our results show that Fung's model also provided the same level of fitting efficiency as the three-parameter exponential model. Table 3 shows the parameters used for Fung's model, and Fig. 4 shows the comparison of force controlled experimental data with Fung's model predicted stress values. Note that second Piola-Kirchhoff stress vs. Green strain are used in Fung's model (Fung, 1993; Huang, 2004; Sun and Sacks, 2005). We have carefully converted our force and displacement data using deformation gradients to generate second Piola-Kirchhoff stress and Green strain suited for the Fung's model. The parameters presented in Table 3 do not need any kinematic conversion when implementing into ABAQUS.

Data from seven tissue specimens for each testing ratio were averaged and fitted against Fung's model (as shown in Fig. 4A-C) resulting in the parameters given in Table 3. No single specimen was able to withstand all of the testing ratios (i.e. 1:1, 1:3, and 3:1) consecutively, therefore it was impossible to represent all three testing ratios with a single parameter set, whereas the three parameter exponential model predicts all the testing ratios using one set of parameters to an acceptable extent. Fig. 4A-C presents data up to a Green strain of 1.5, which is

equivalent to a 70% true strain for simplicity in comparison to the displacement controlled tests fitted with the exponential model, where the tearing strain was found to be about 70%. However, it is important to note that the maximum tension of 200 N/m led to strains higher than 70% for the compliant radial direction of the tissue in some tests. The parameters obtained in Table 3 are currently used in the finite element analysis in our ongoing study. In all of the models presented, we also provide one single set of parameters to represent the tissue behaviors to use in a finite element method implementation, as shown in Tables 1 and 2.

There are some limitations to the study as well, which may counteract the better predictive power of the phenomenological models. First, to facilitate an understanding of venous valve tissue behavior, we have chosen to use previously established models from the literature to investigate how well they might apply to the tissue under study. Due to the differences (or similarities) in response curves for valve tissue (or wall tissue) compared to the published literature, using the same functional expressions proved useful to a certain extent. However, changing the exponents for I_1 and α in the expression may provide better results for the phenomenological models. The biggest implicit assumption of this framework was the high unidirectional alignment of fibers and further aligning of the fiber axis perfectly with the loading axis. A perfect fiber axis may or may not exist and can vary slightly from sample to sample, which can only be taken into account by studying the structure of each sample before testing. Also, the alignment of the fiber and loading axes involves mounting the sample on the mechanical tester and is prone to human error. A small deviation can alter the experimental data greatly. Presently, our equipment does not have the capability of measuring any shear stress which might occur during testing. Great care has been taken while mounting the samples so that the rakes align perfectly, but a misalignment in the rakes could be responsible for erroneous measurements and model predictions. Moreover, since the models are phenomenological in nature, it is difficult to relate the material parameters directly to a physical attribute of the tissue. Therefore, while this model gives a good start to the study of jugular venous tissue, it can also support any structurally motivated future studies. The study also provides investigators with representative material parameters to form a continuum model when such is required for numerical analyses and computational simulations, which may be of great help during the primary stages of bioprosthetic designs, valve-replacement surgeries, and when investigating valvular diseases.

4. Conclusion

The primary aim of the study was to constitutively model the behavior of jugular vein wall tissue and valve leaflet tissue. Towards this end, response curves were generated using numerical mathematical framework to calculate W_1 and W_α based on the constant invariant testing as put forward by Humphrey et al. (1990a, 1990b). The behavior of partial derivatives of strain energy came out almost linear in the case of wall tissue (proximal and distal alike) and highly non-linear in case of valve leaflet tissue. To explain this behavior, we selected two different strain energy descriptors from the literature – Non-linear polynomial to explain the behavior of wall (Eq. 2) and an exponential behavior to best explain the characteristics of the valve leaflet tissue (Eq. 3). Model parameters were calibrated based on additional sets of equibiaxial and off axis biaxial testing for both energy descriptors. The

Table 3
Material parameters for the valve tissue using Fung's model.

| Test Ratio | C (MPa) | A ₁ | A ₂ | A ₃ | A ₄ | A ₇ | A ₈ | A ₉ | A ₁₀ | A ₁₁ | R _x | R _y |
|------------|---------|----------------|----------------|----------------|----------------|----------------|----------------|----------------|-----------------|-----------------|----------------|----------------|
| 1:1 | 4.020 | 0.086 | 0.055 | 0.127 | 0 | 0.112 | 0.063 | 0.010 | 0 | 0 | 0.976 | 0.961 |
| 3:1 | 1.098 | 1.605 | 0.246 | 0 | 0 | 0.7513 | 0.478 | 0.001 | 0 | 0 | 0.973 | 0.962 |
| 1:3 | 5.706 | 0 | 0.056 | 0.041 | 0 | 0.030 | 0.024 | 0.001 | 0 | 0 | 0.986 | 0.976 |

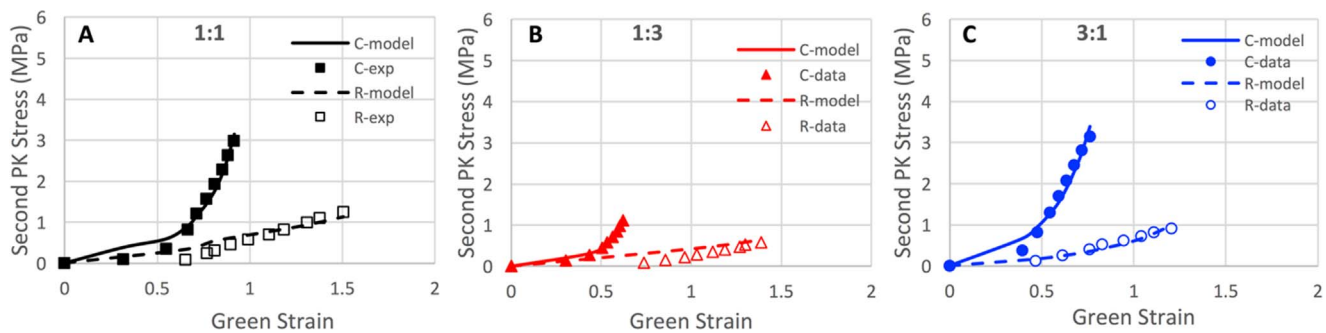


Fig. 4. Second Piola-Kirchhoff (PK) stress vs Green strain with fitting curves using Fung's model.

individual fits were near perfect for the wall tissue, whereas in case of the model predictions for valves, a consistent prediction error was observed in circumferential direction in off-axis radial (2:1) stretch protocol for all the valve samples as can be seen in Fig. 3. Using the remaining test samples, Fung's model provided the same level of correlation between the experimental data and model predicted data for the valve tissue. These results from the current study can be helpful in offering insight into the mechanical behavior of soft tissues. This study can fill a critical gap in the basic science of venous tissues, as well as serve as a springboard for innovation, informing approaches to the treatment of venous valve diseases such as chronic venous insufficiency by providing a framework for future finite element simulations.

Acknowledgement

This research was supported by the NSF CBET1553430. The authors are thankful to Adam Benson for his help with part of the experimental work.

References

- Ackroyd, J.S., Pattison, M., Browse, N.L., 1985. A study of the mechanical properties of fresh and preserved human femoral vein wall and valve cusps. *Br. J. Surg.* 72, 117–119.
- Arruda, E.M., Boyce, M.C., 1993. A 3-dimensional constitutive model for the large stretch behavior of rubber elastic-materials. *J. Mech. Phys. Solids* 41, 389–412.
- Bergan, J.J., 2008. Venous valve incompetence: the first culprit in the pathophysiology of chronic venous insufficiency. *Medicographia* 30, 87–94.
- Bernardini, E., De Rango, P., Piccioli, R., Bisacci, C., Pagliuca, V., Genovese, G., Bisacci, R., 2010. Development of primary superficial venous insufficiency: the ascending theory. *Obs. hemodynamic Data a 9-year Exp. Ann. Vasc. Surg.* 24, 709–720.
- Billiar, K.L., Sacks, M.S., 2000. Biaxial mechanical properties of the natural and glutaraldehyde treated aortic valve cusp-Part I: experimental results. *J. Biomech. Eng.* 122, 23–30.
- Buescher, C.D., Nachiappan, B., Brumbaugh, J.M., Hoo, K.A., Janssen, H.F., 2005. Experimental studies of the effects of abnormal venous valves on fluid flow. *Biotechnol. Progress.* 21, 938–945.
- Eberhardt, R.T., Raffetto, J.D., 2005. Chronic venous insufficiency. *Circulation* 111, 2398–2409.
- Edwards, J.E., Edwards, E.A., 1940. The saphenous valves in varicose veins. *Am. Heart J.* 19, 338.
- Eilaghi, A., Flanagan, J.G., Brodland, G.W., Ethier, C.R., 2009. Strain Uniformity in Biaxial Specimens is Highly Sensitive to Attachment Details. *J. Biomech. Eng. Trans. ASME* 131, 091003-091003.
- Eilaghi, A., Flanagan, J.G., Tertinegg, I., Simmons, C.A., Brodland, G.W., Ethier, C.R., 2010. Biaxial mechanical testing of human sclera. *J. Biomech.* 43, 1696–1701.
- Fung, Y.C., 1965. *Foundations of Solid Mechanics*. Prentice-Hall, Englewood Cliffs.
- Fung, Y.C., 1993. *Biomechanics: Mechanical Properties of Living Tissues*. Springer Verlag, New York.
- Gent, A.N., 1996. A new constitutive relation for rubber. *Rubber Chem. Technol.* 69, 59–61.
- Gent, A.N., Thomas, A.G., 1958. Forms for the stored (strain) energy function for vulcanized rubber. *J. Polym. Sci.* 28, 625–628.
- George, J.S., 2012. Evaluation and treatment of lower extremity superficial venous insufficiency. *Northeast Fla. Med.* 63, 23–28.
- Gottlob, R., May, R., 1986. *Venous Valves: Morphology, Function, Radiology, Surgery*. Springer-Verlag, Wien; New York.
- Holzappel, G.A., Gasser, T.C., Ogden, R.W., 2000. A new constitutive framework for arterial wall mechanics and a comparative study of material models. *J. Elast.* 61, 1–48.
- Holzappel, G.A., Gasser, T.C., Ogden, R.W., 2004. Comparison of a multi-layer structural model for arterial walls with a fung-type model, and issues of material stability. *J. Biomech. Eng. Trans. ASME* 126, 264–275.
- Huang, H.-Y.S., 2004. *Micromechanical Simulations of Heart Valve Tissues*. University of Pittsburgh, Pittsburgh, pp. 283.
- Huang, H.-Y.S., Balhouse, B.N., Huang, S., 2012. Application of simple biomechanical and biochemical tests to heart valve leaflets: implications for heart valve characterization and tissue engineering. *Proc. Inst. Mech. Eng. Part H-J. Eng. Med.* 226, 868–876.
- Huang, S., Huang, H.-Y.S., 2015. Biaxial Stress Relaxation of Semilunar Heart Valve Leaflets during Simulated Collagen Catabolism: Effects of Collagenase Concentration and Equibiaxial Strain-State. In: *Proceedings of the Institution of Mechanical Engineers, Part H: Journal of Engineering in Medicine* 229, pp. 721–731.
- Huang, H.Y.S., Lu, J., 2017. Biaxial mechanical properties of bovine jugular venous valve leaflet tissues. *Biomech. Model. Mechanobiol.* First Online. <http://dx.doi.org/10.1007/s10237-017-0927-1>. <https://link.springer.com/article/10.1007/s10237-017-0927-1>.
- Humphrey, J.D., 1999. An evaluation of pseudoelastic descriptors used in arterial mechanics. *J. Biomech. Eng. Trans. ASME* 121, 259–262.
- Humphrey, J.D., 2002. *Cardiovascular Solid Mechanics: Cells, Tissues, and Organs*. Springer, New York.
- Humphrey, J.D., Strumpf, R.K., Yin, F.C., 1990a. Determination of a constitutive relation for passive myocardium: I. A new functional form. *J. Biomech. Eng.* 112, 333–339.
- Humphrey, J.D., Strumpf, R.K., Yin, F.C., 1990b. Determination of a constitutive relation for passive myocardium. 2. Parameter-estimation. *J. Biomech. Eng. Trans. ASME* 112, 340–346.
- Kaul, N., 2016. *Constitutively Model and Compare the Structural-Mechanical Properties of Jugular Vein Tissue, Mechanical and Aerospace Engineering*. North Carolina State University, Raleigh. <https://repository.lib.ncsu.edu/handle/1840.20/33239>.
- Lu, J., 2016. *Biaxial Mechanical Properties of Venous Valve Leaflet Tissues, Mechanical and Aerospace Engineering*. North Carolina State University, Raleigh. <https://repository.lib.ncsu.edu/handle/1840.16/10980>.
- Martin, C., Sun, W., 2014. Simulation of long-term fatigue damage in bioprosthetic heart valves: effects of leaflet and stent elastic properties. *D - 101135325 13*, pp. 759–770.
- Masoumi, N., Jean, A., Zugates, J.T., Johnson, K.L., Engelmayer, G.C., 2013. Laser micro-fabricated poly(glycerol sebacate) scaffolds for heart valve tissue engineering. *J. Biomed. Mater. Res. Part A* 101, 104–114.
- May-Newman, K., Lam, C., Yin, F.C.P., 2009. A hyperelastic constitutive law for aortic valve tissue. *J. Biomech. Eng. Trans. ASME* 131.
- May-Newman, K., Yin, F.C., 1998. A constitutive law for mitral valve tissue. *J. Biomech. Eng.* 120, 38–47.
- Mooney, M., 1940. A theory of large elastic deformation. *J. Appl. Phys.* 11, 582–592.
- Nguyen, T.D., Jones, R.E., Boyce, B.L., 2008. A nonlinear anisotropic viscoelastic model for the tensile behavior of the corneal stroma. *J. Biomech. Eng. Trans. ASME* 130.
- Nolan, D.R., Gower, A.L., Destrade, M., Ogden, R.W., McGarry, J.P., 2014. A robust anisotropic hyperelastic formulation for the modelling of soft tissue. *J. Mech. Behav. Biomed. Mater.* 39, 48–60.
- Nolan, D.R., McGarry, J.P., 2016. On the correct interpretation of measured force and calculation of material stress in biaxial tests. *J. Mech. Behav. Biomed. Mater.* 53, 187–199.
- Ogden, R.W., 1972. Large deformation isotropic elasticity - correlation of theory and experiment for incompressible rubberlike solids. In: *Proceedings of the Royal Society of London Series A-Mathematical and Physical Sciences*, 326, pp. 565–& .
- Press, W.H., Flannery, B., Teukolsky, S.A., Vetterling, W.T., 1992. *Numerical Recipes in C: The Art of Scientific Computing*. Cambridge University Press, Cambridge.
- Rivlin, R.S., 1948a. Large elastic deformations of isotropic materials. 1. Fundamental concepts. *Philos. Trans. R. Soc. Lond. Ser. A-Math. Phys. Sci.* 240, 459–508.
- Rivlin, R.S., 1948b. Large elastic deformations of isotropic materials. 4. Further developments of the general theory. *Philos. Trans. R. Soc. Lond. Ser. A-Math. Phys. Sci.* 241, 379–397.
- Rivlin, R.S., Saunders, D.W., 1951. Large elastic deformations of isotropic materials, VII. Experiments on the deformation of rubber. *Philos. Trans. R. Soc. A243*, 251–288.
- Shariff, M., 2000. Strain energy function for filled and unfilled rubberlike material. *Rubber Chem. Technol.* 73, 1–18.
- Slaughter, W.S., 2001. *The Linearized Theory of Elasticity*. Birkhauser, Boston.
- Sun, W., Sacks, M.S., 2005. Finite element implementation of a generalized Fung-elastic constitutive model for planar soft tissues. *Biomech. Model. Mechanobiol.* 4, 190–199.
- Treloar, L.R.G., 1943a. The elasticity of a network of longchain molecules - II. *Trans. Faraday Soc.* 39, 0241–0246.
- Treloar, L.R.G., 1943b. The elasticity of a network of longchain molecules. I. *Trans. Faraday Soc.* 39, 0036–0041.
- Treloar, L.R.G., 1946. The statistical length of long-chain molecules. *Trans. Faraday Soc.* 42, 77–82.
- Vogel, D., Walsh, M.E., Chen, J.T., Comerota, A.J., 2012. Comparison of vein valve function following pharmacomechanical thrombolysis versus simple catheter-directed thrombolysis for iliofemoral deep vein thrombosis. *J. Vasc. Surg.* 56, 1351–1354.
- Yin, F.C.P., Chew, P.H., Zeger, S.L., 1986. An approach to quantification of biaxial tissue stress-strain data. *J. Biomech.* 19, 27–37.